2002

Coherent Integration of 0.5 GHz Spectral Holograms at 1536 Nm Using Dynamic Biphase Codes

Z Cole

Thomas Böttger
University of San Francisco, tbottger@usfca.edu

R Krishna Mohan

R Reibel

W R. Babbitt

See next page for additional authors

Recommended Citation

Z. Cole, T. Böttger, R. Krishna Mohan, R. Reibel, W. R. Babbitt, R. L. Cone, and K. D. Merkel. Coherent integration of 0.5 GHz spectral holograms at 1536 nm using dynamic bi-phase codes. Applied Physics Letters 81, 3525 (2002). http://dx.doi.org/10.1063/1.1518152

Authors
Z Cole, Thomas Böttger, R Krishna Mohan, R Reibel, W R. Babbitt, R L. Cone, and K D. Merkel

Coherent integration of 0.5 GHz spectral holograms at 1536 nm using dynamic biphase codes

Z. Cole, T. Böttger, R. Krishna Mohan, R. Reibel, W. R. Babbitt, R. L. Cone, and K. D. Merkel

Citation: Applied Physics Letters **81**, 3525 (2002); doi: 10.1063/1.1518152
View online: http://dx.doi.org/10.1063/1.1518152
View Table of Contents: http://scitation.aip.org/content/aip/journal/apl/81/19?ver=pdfcov
Published by the AIP Publishing

Coherent integration of 0.5 GHz spectral holograms at 1536 nm using dynamic biphase codes

Z. Cole, T. Böttger, R. Krishna Mohan, R. Reibel, W. R. Babbitt, R. L. Cone, and K. D. Merkel[a)]
Spectrum Lab and Physics Department, Montana State University, Bozeman, Montana 59717

(Received 5 June 2002; accepted 9 September 2002)

Spectral hole-burning-based optical processing devices are proposed for coherent integration of multiple high-bandwidth interference patterns in a spectral hole-burning medium. In this implementation, 0.5 GHz spectral holographic gratings are dynamically accumulated in $Er^{3+}:Y_2SiO_5$ at 4.2 K using a 1536 nm laser frequency stabilized to a spectral hole, along with commercial off-the-shelf components. The processed data, representing time delays over 0.5–2.0 μs, were optically read out using a frequency-swept probe; this approach makes possible the use of low-bandwidth, large-dynamic-range detectors and digitizers and enables competitive processing for applications such as radar, lidar, and radio astronomy. Coherent integration dynamics and material advances are reported. © *2002 American Institute of Physics.*
[DOI: 10.1063/1.1518152]

Analog optical signal processing devices based on spectral hole-burning techniques in rare-earth-doped crystals have been proposed and demonstrated, providing instantaneous bandwidths over 10 GHz, correlation time lengths of several microseconds, millisecond integration times, and large dynamic range. Applications, to date, include optical storage,[1,2] processing,[3,4] true-time delay,[5] rf spectrum analysis,[6] and quantum computing,[7] among others. In previous processing demonstrations, spatial–spectral holographic gratings were recorded and then coherently probed to stimulate the emission of an optical coherent transient signal representing the processed output. This letter proposes and demonstrates a spectral holographic processor, where signal processing occurs during the recording stage of a spectral hologram and readout of the processed data is accomplished using a frequency-swept probe and low bandwidth detection.

This approach enables spectral hole-burning-based processing applications including radar (discussed here), lidar, and radio astronomy. In radar range and Doppler processing, a coded rf waveform is transmitted, reflected by a target, and then received along with additive noise after a delay, τ_D. The delay can be accurately determined by modulating the transmitted and returned rf waveforms onto an optical carrier and illuminating a spectral hole-burning material, which acts as a correlative signal processor. For a single processing shot, two time-ordered waveforms resonantly interfere in a frequency selective inhomogeneously broadened transition, resulting in a frequency dependent population grating (i.e., a spectral holographic grating) that includes the spectral product of the waveforms modified by a $1/\tau_D$ periodic component.[1] The processed information persists for and may be readout within the transition lifetime T_1. For multishot processing, with pulse repetition frequency of $1/\tau_{\mathrm{Rep}}$, up to T_1/τ_{Rep} shots may be coherently integrated by the medium, given sufficient laser frequency stability over T_1, resulting in an accumulated spectral grating.[8] For N coherent shots, all having a common delay, the primary $1/\tau_D$ grating component accumulates as $\sim N^{2\alpha}$, where $\alpha \lesssim 1$ for small N. For large N, the integration gain saturates due to population dynamics. For agile radar processing applications, where each transmitted waveform is a unique code, the material coherently integrates the processing sequence, recording a dynamically accumulated spectral grating.[9] The primary $1/\tau_D$ component accumulates while the changing spectral features of the dynamic codes and additive noise are averaged. Coherent integration of spectral gratings is achieved with low optical input power at pulse repetition frequencies of 1 kHz to 1 MHz with presently available materials near 1550 nm and 800 nm. Further, Doppler processing is achieved by introducing multiple optical frequency shifted copies of the transmitted waveform into different spatial channels of the material and parallel processing the returned signal (nonshifted) in all channels. Accumulation of the $1/\tau_D$ grating component occurs only when the frequency shift closely matches the Doppler shift on the return signal.[10] The reconfiguration of a spectral grating in a single spatial location is limited by T_1.

In this letter, we experimentally demonstrate coherent integration of up to 800 shots over 0.5 GHz bandwidth at 1536 nm in an $Er^{3+}:Y_2SiO_5$ crystal maintained at 4.2 K. Each transmit waveform was a 200-bit long binary-phase-shift-keyed code. The code time-bandwidth product is a factor of ~7 higher than previous spectral holographic processing efforts.[3] A frequency-swept probe measured processed time delays ranging from 0.5 to 2.0 μs. We report coherent integration dynamics and material parameters under these conditions. This demonstration utilized technologies developed through Montana State University collaborations, including a laser, frequency stabilized to a transient spectral hole[11] and a rare-earth-doped spectral hole-burning crystal,[12] along with commercial components. In the processing sequence, a shot consisted of a randomly generated zero-mean waveform $S_1^n(t)$ and its time-delayed replica $S_2^n(t)=S_1^n(t-\tau_D)$, emulating a radar transmit and return waveform pair

[a)]Author to whom correspondence should be addressed; electronic mail: merkel@spectrum.montana.edu

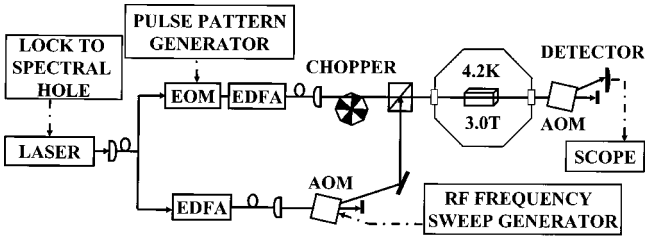

FIG. 1. Experimental schematic is shown: EOM—electro-optic modulator; EDFA—erbium-doped fiber amplifier; and AOM—acousto-optic modulator.

without additive noise. Shots were introduced at a repetition interval τ_{Rep}, with a fixed delay τ_D for $n=1,2,...N$. To avoid coherent beating between consecutive shots, we set $\tau_{\mathrm{Rep}} \geqslant 2T_2$, where T_2 is the coherence time of the transition.

We implemented a frequency-swept readout technique to probe the grating structure by frequency dependent transmission,[13] rather than using the traditional brief pulse to stimulate a photon echo. The transmitted signal can be detected, digitized, and postprocessed to extract the processed delay(s). Frequency-swept probing enables practical system development, with the following advantages: (1) use of currently available low bandwidth, large dynamic range detectors ($\sim$1 MHz and $\sim$120 dB), and digitizers ($\sim$2.5 MS/s and $\sim$16 bit) to extract delay information from high bandwidth gratings, and (2) use of low power lasers with electro-optic frequency tuning elements[14] to provide reproducible, high-bandwidth frequency-swept probes. The frequency-sweep rate should be less than $1/(\tau_{D_{\max}})^2$ to ensure sufficient temporal resolution, where $\tau_{D_{\max}}$ is the maximum resolvable delay limited by T_2. The required bandwidth of detection is just $1/\tau_{D_{\max}}$ rather than the signal bandwidth B. The required sweep duration is $[B\cdot(\tau_{D_{\max}})^2]$. For example, if $\tau_{D_{\max}}=1.0\ \mu$s, a sweep rate of 1.0 MHz/μs and a detection bandwidth of 1 MHz$\ll B$ is sufficient.

Experiments were performed in a 2 mm thick 0.005 at.% $Er^{3+}:Y_2SiO_5$ crystal grown by Scientific Materials Corporation, with $\alpha L=1.8$ at the 1536.14 nm line center. The ${}^4I_{15/2}(1)\rightarrow{}^4I_{13/2}(1)$ transition of site 1 had a 0.5 GHz absorption profile. The integration time for the holographic processor is set by $T_1=11$ ms, the population lifetime of the excited state of the Er^{3+} ions.[15] Material studies determined the optimum direction for an applied magnetic field to minimize the effects of spectral diffusion on the holographic grating.[15] When a 3.0 T external field was applied parallel to the $\mathbf{D}_1$ axis, operation was practical at 4.2 K, a temperature that can be provided by closed-cycle cryocooler technology. The external cavity diode laser was stabilized to a regenerative spectral hole in a different spatial region of the same crystal.[11] The stabilization occurs at the required wavelength and provides the required stability over T_1. Thus, the processing and stabilization techniques can be transferred to other hole burning materials.[12] The spectral hole was nominally 30 kHz wide and frequency stability of $\sim$1 kHz (Allan deviation over an integration time of 10 ms) was achieved. Both processing and stabilization beams propagated parallel to the crystal **b** axis and were polarized along $\mathbf{D}_2$.

Figure 1 depicts the main experimental components. The stabilized laser—tuned to the absorption line center—was fiber coupled and split into a processing and probing beam.

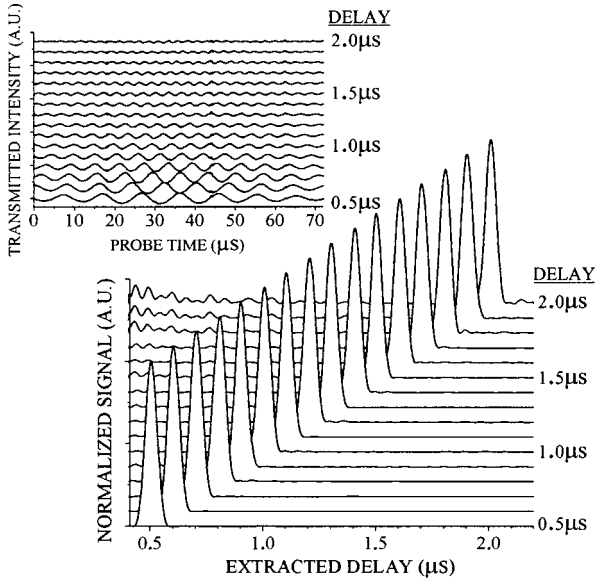

FIG. 2. Normalized traces of extracted time delay data are shown for processed time delay τ_D values ranging from 0.5–2.0 μs, after 800 shots using a 25 mW processing beam. The inset shows traces of the frequency-swept probe, which map the corresponding accumulated spectral gratings.

The processing beam was continuously biphase-shift-keyed modulated by an electro-optic phase modulator driven by a pulse pattern generator and then amplified. Each S^n was modulated at 0.5 Gb/s. Between all S^n, the light was square wave modulated (...101010...) at 1 Gb/s. A chopper created a 4 ms off window in the processing beam to allow for probing 0.5 ms into this window. The probing beam was amplified and frequency swept by an acousto-optic modulator. The beams were made collinear and focused to a $\sim$50 μm ($1/e^2$ diameter) spot in the crystal. The transmitted probe was deflected toward a 125 MHz bandwidth, $\sim$50 dB dynamic range photodetector.

For all experiments, each waveform was 400 ns long (200 bits at 2 ns/bit) with $\tau_{\mathrm{Rep}}=5\ \mu$s. The probe pulse was 10 μW and swept over $\sim$15 MHz, shifted 165 MHz from the carrier at a sweep rate of 0.2083 MHz/μs. Postprocessing of the transmitted probe consisted of filtering to minimize the low-frequency components of the unabsorbed probe envelope, performing a fast Fourier transform, and calculating its magnitude squared. Figure 2 plots postprocessed data for $N=800$ shots, where τ_D was varied from 0.5 to 2.0 μs in 0.1 μs increments using a 25 mW programming beam. The primary peak of each trace was normalized to the 0.5 μs peak. Analysis of the peaks, representing the extracted time delays, showed an arrival time accuracy of $\sim$3 ns. The inset of Fig. 2 shows corresponding traces of the filtered transmitted probe, revealing the periodic $1/\tau_D$ structure and reduced grating strength with increasing delays due to coherence decay. For 25 mW and 40 mW excitation, a first-order fit of the non-normalized peaks to $\exp(-2\tau_D/T_2)$ results in a T_2 value of $0.82\pm0.03\ \mu$s for these conditions.

Figure 3(a) plots two examples of signal strength (log scale) versus extracted time delay (linear scale) when $\tau_D=0.5\ \mu$s and $N=200$ for 25 mW (thin line) and 40 mW (bold line) programming powers. In addition to the primary delay, there are nonlinear terms, or spurs, resulting in harmonics of each delay (and intermods if there are multiple

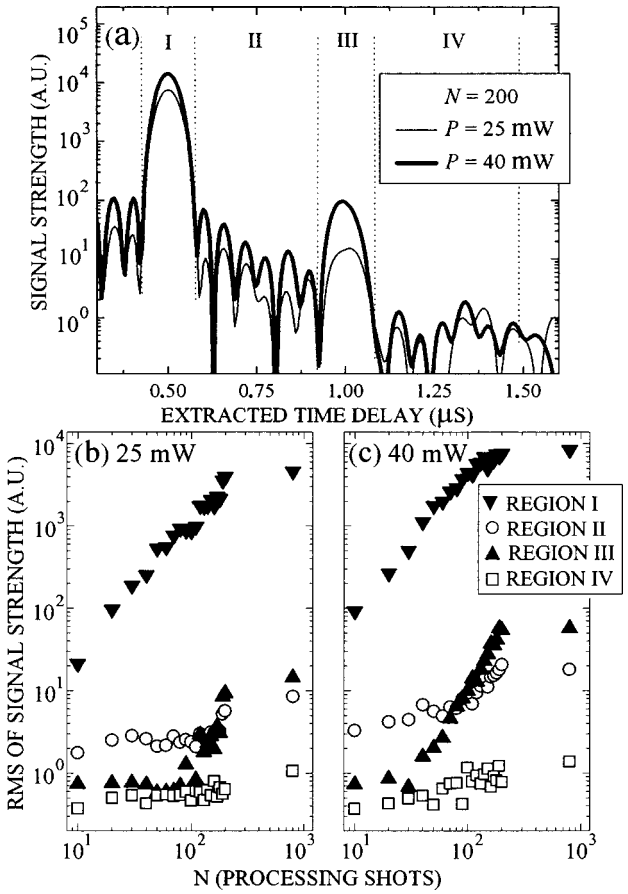

FIG. 3. (a) Traces of the extracted time delay are shown (log scale) for processed time delay $\tau_D = 0.5\ \mu$s after $N = 200$ shots for 25 mW pulses (thin trace) and 40 mW pulses (bold trace). The data has four regions of interest: (I) the primary peak; (II) the right-hand side sidelobe region; (III) the second harmonic of the primary peak; and (IV) the background noise of the system. rms values of regions I–IV vs N are shown in (b) for 25 mW and (c) for 40 mW programming pulses over a 4 ms integration time.

delays). The second-harmonic observed here accumulates as $N^{4\beta}$. The grating strength and α and β depend on N, the optical programming power, coherence loss $[\propto \exp(-2\tau_D/T_2)]$ during each shot, and population decay $[\propto \exp(-\tau_{\mathrm{Rep}}/T_1)]$ between shots. In Fig. 3(a), the primary peak and its second harmonic can be clearly observed and as expected increase with input power. Figure 3(a) is divided into four regions: I contains the primary peak representing the time delay τ_D; II contains the right temporal correlation sidelobes; III contains the second harmonic of the primary peak; and IV contains the system background noise. There are residual low-frequency components due to imperfect postprocessing of the unabsorbed probe, limiting absolute comparison between the regions in this demonstration; we are, therefore, not including the left temporal sidelobe regions in our analysis. The peak temporal width of ~ 65 ns (full width at half maximum) is set by the probe bandwidth.

Figures 3(b) and 3(c) plot the root-mean-square (rms) values for regions I–IV (log scale) versus N (log scale) for a fixed $\tau_D = 0.5\ \mu$s with (b) 25 mW or (c) 40 mW programming power. In Fig. 3(c), the higher programming power exhibits larger grating strength and stronger nonlinearities, as expected. Region I peaks of both Figs. 3(b) and 3(c) increase as $2\alpha \sim 1.8$ for the first 100 shots. The second harmonics in region III of Fig. 3(b) and 3(c) rise above the noise floor at $N = 70$ and $N = 30$, respectively, and both grow (for $N \leqslant 200$) as $4\beta \sim 2.4$. The relatively flat nature of region II, particularly for the first 100 shots of Fig. 3(b), highlights the effects of coherent integration with dynamic codes. Improved performance is expected with wider bandwidth frequency-swept sources,[14] detectors with larger dynamic range, and materials with higher bandwidths and longer coherence times.

Adoption of these techniques offers the following for analog signal processing applications: (1) high bandwidth, large time–bandwidth product, and large dynamic range operation without high-bandwidth detectors and digitizers, (2) the ability to process waveforms that change from shot to shot, (3) coherent integration of up to $\sim T_1/\tau_{\mathrm{Rep}}$ shots, or of two continuous signals correlated over a T_2 window for a time T_1, and (4) Doppler processing.

In summary, dynamic accumulation of spectral holographic gratings by coherent integration of up to 800 shots was demonstrated. The signal processing bandwidth was 0.5 GHz, limited by the crystal used, but could exceed 10 GHz using currently available crystals and modulators. Time delays of 0.5 to 2.0 μs were processed and extracted with 3 ns accuracy. The demonstration used a stabilized diode laser, 1550 nm telecom components, and a frequency-swept probe. Successful processing and frequency stabilization in crystals at 4.2 K make possible the use of closed-cycle cryocoolers, and enable practical, high performance, multi-GHz, analog correlative processors using spectral holography.

This collaboration was supported by AFOSR (Grants F49620-00-1-314 and F49620-00-1-0313), NASA Ames (Grant NAG2-1323), and by the University of Colorado MURI program (Grant N00014-97-1-1006). The authors thank Kelvin Wagner at the University of Colorado, for many helpful discussions.

[1] T. W. Mossberg, Opt. Lett. **7**, 77 (1982).
[2] A. Renn, U. P. Wild, and A. Rebane, J. Phys. Chem. A **106**, 3045 (2002), and references therein.
[3] T. L. Harris, Y. Sun, W. R. Babbitt, R. L. Cone, J. A. Ritcey, and R. W. Equall, Opt. Lett. **25**, 85 (2000), and references therein.
[4] K. D. Merkel, Z. Cole, and W. R. Babbitt, J. Lumin. **86**, 375 (2000), and references therein.
[5] R. Reibel, Z. Barber, M. Tian, and W. R. Babbitt, Opt. Lett. **27**, 494 (2002), and references therein.
[6] L. Menager, I. Lorgere, J. L. Le-Gouet, D. Dolfi, and J. P. Huignard, Opt. Lett. **26**, 1245 (2001), and references therein.
[7] N. Ohlsson, R. Krishna Mohan, and S. Kröll, Opt. Commun. **201**, 71 (2002).
[8] K. D. Merkel, R. D. Peters, P. B. Sellin, K. S. Repasky, and W. R. Babbitt, Opt. Lett. **25**, 1627 (2000), and references therein.
[9] In radio astronomy applications the signals are inherently dynamic.
[10] Kelvin Wagner (private communication).
[11] P. B. Sellin, N. M. Strickland, T. Böttger, J. L. Carlsten, and R. L. Cone, Phys. Rev. B **63**, 155111 (2001).
[12] Y. Sun, T. Böttger, C. W. Thiel, R. L. Cone, and R. W. Equall (unpublished).
[13] C. M. Jefferson and A. J. Meixner, Chem. Phys. Lett. **189**, 60 (1992).
[14] L. Levin, Opt. Lett. **27**, 237 (2001), and references therein.
[15] T. Böttger, Y. Sun, G. J. Pryde, G. Reinemer, and R. L. Cone, J. Lumin. **94**, 565 (2001).